Light responses and light adaptation in rat retinal rods at different temperatures

S. Nymark[1], H. Heikkinen[1], C. Haldin[2], K. Donner[2] and A. Koskelainen[1]

[1] *Laboratory of Biomedical Engineering, Helsinki University of Technology, FI-02015 HUT, Finland*
[2] *Department of Biological and Environmental Sciences, University of Helsinki, FI-00014, Finland*

Rod responses to brief pulses of light were recorded as electroretinogram (ERG) mass potentials across isolated, aspartate-superfused rat retinas at different temperatures and intensities of steady background light. The objective was to clarify to what extent differences in sensitivity, response kinetics and light adaptation between mammalian and amphibian rods can be explained by temperature and outer-segment size without assuming functional differences in the phototransduction molecules. Corresponding information for amphibian rods from the literature was supplemented by new recordings from toad retina. All light intensities were expressed as photoisomerizations per rod (Rh*). In the rat retina, an estimated 34% of incident photons at the wavelength of peak sensitivity caused isomerizations in rods, as the (hexagonally packed) outer segments measured 1.7 μm × 22 μm and had specific absorbance of 0.016 μm^{-1} on average. Fractional sensitivity (S) in darkness increased with cooling in a similar manner in rat and toad rods, but the rat function as a whole was displaced to a *ca* 0.7 log unit higher sensitivity level. This difference can be fully explained by the smaller dimensions of rat rod outer segments, since the same rate of phosphodiesterase (PDE) activation by activated rhodopsin will produce a faster drop in cGMP concentration, hence a larger response in rat than in toad. In the range 15–25°C, the waveform and absolute time scale of dark-adapted dim-flash photoresponses at any given temperature were similar in rat and toad, although the overall temperature dependence of the time to peak (t_p) was somewhat steeper in rat ($Q_{10} \approx 4$ *versus* 2–3). Light adaptation was similar in rat and amphibian rods when measured at the same temperature. The mean background intensity that depressed S by 1 log unit at 12°C was in the range 20–50 Rh* s^{-1} in both, compared with *ca* 4500 Rh* s^{-1} in rat rods at 36°C. We conclude that it is not necessary to assume major differences in the functional properties of the phototransduction molecules to account for the differences in response properties of mammalian and amphibian rods.

(Resubmitted 16 May 2005; accepted after revision 14 July 2005; first published online 21 July 2005)
Corresponding author S. Nymark: Laboratory of Biomedical Engineering, Helsinki University of Technology, PO Box 2200, FI-02015 HUT, Finland. Email: soile.nymark@hut.fi

The phototransduction cascade and its regulatory mechanisms are basically similar in all rod photoreceptors that have been studied (see Pugh & Lamb, 2000). On the other hand, quantitative parameters of amplification, activation and deactivation kinetics, and light adaptation derived from the electrical responses to light differ so as to suggest important differences in the functioning of the phototransduction molecules in mammals and 'lower vertebrates' (commonly represented by amphibians). The rods of both classes can respond reliably to a single photon, but the initial amplification rate in mammalian rods is higher by two orders of magnitude and the response peaks at a much earlier time after photon absorption (Baylor *et al.* 1979*b*, 1984; Matthews, 1991; Robinson *et al.* 1993; Kraft *et al.* 1993; Nikonov *et al.* 2000). Although mammalian rods, including those of humans, do have the capacity to light adapt, i.e. reset sensitivity depending on the average illumination level, adaptation is normally effective only in a narrow range of high light intensities (Tamura *et al.* 1989; Matthews, 1991; Hood & Birch, 1993; Kraft *et al.* 1993; Silva *et al.* 2001; Friedburg *et al.* 2001). By contrast, amphibian rods exhibit extensive adaptation starting at very low light intensities (Fain, 1976; Hemilä, 1977; Baylor *et al.* 1980; Donner *et al.* 1990*a*).

These differences do not necessarily indicate differences in the functional properties of the transduction proteins. The data being compared are affected by differences in two simple physical factors certain to be important, temperature and outer-segment size (cf. Pugh & Altman, 1988; Arshavsky *et al.* 2002). Experiments on mammals

 DOI: 10.1113/jphysiol.2005.090662

and amphibians have, with few exceptions, been conducted at very different temperatures (typically, 37°C *versus* 20°C or less), and the outer segment (OS) of a sturdy amphibian rod may be some 50 times larger in volume than that of a slender mammalian rod.

The purpose of the present work was to assess how far quantitative differences between mammalian and amphibian rod photoresponses can be explained by temperature and OS size. Most of the experiments reported here concern effects of temperature on rat rods, but some parallel measurements were carried out in toad rods to supplement amphibian data from the literature. As the cells were subjected to wide and largely unnatural temperature changes, it was particularly important that their physiological condition would be as 'natural' as possible in other respects. Rods *in situ* in retinal tissue have been found to retain at least their capacity for light adaptation much better than isolated rods in suction-pipette experiments (Donner *et al.* 1990*a*). Therefore, the preparation used was the intact, isolated retina, where transretinal ERG allowed long and stable recording of population photoresponses from rods over a temperature range extending from rat body temperature (36°C) down to 5°C.

We find that most of the differences between photoresponses of rat and toad rods disappear when they are compared at the same temperature. The major remaining difference is the overall level of fractional sensitivity in the dark-adapted state, which at any given temperature was 5–6 times higher in rat. In the model we use for analysis of photoresponses (Fain *et al.* 2001), this difference is captured by a parameter associated with the initial rate of cGMP hydrolysis, which in terms of concentration change will be inversely proportional to cytoplasmic volume. The average rod OS volume of the rat is estimated to be 39 times smaller than that of the toad, and in the model this factor alone suffices to explain the faster [cGMP] drop in rat rods.

Methods

Preparation, recording and light stimulation

Rat experiments. Wistar rats (*Rattus norvegicus*) were dark-adapted overnight or for at least 3 h. Use and handling of all the animals in this study were in accordance with the Finland Animal Welfare Act 1986 with guidelines of the Animal Experimentation Committee of the University of Helsinki. The animals were killed by CO_2 inhalation and decapitation, the eyes were enucleated and bisected along the equator, and the retinas were detached in cooled Ringer solution under dim red light. The isolated retina was placed photoreceptors upwards in a specimen holder (Donner *et al.* 1988) where the effective circular measurement area (in direct contact with the lower electrode space) was 1.2 mm in diameter. The whole flat circular area exposed to stimulating light extended 0.4 mm beyond the effective measurement area. Over this area the upper (photoreceptor) side was superfused with a constant flow (*ca* 1.4 ml min^{-1}) of Ringer solution containing (mM): Na^+ 139.7, K^+ 3.3, Mg^{2+} 2.0, Ca^{2+} 1.0; Cl^- 143.2, glucose, 10.0; EDTA, 0.01; Hepes, 12.0. The solution was buffered to pH 7.5–7.7 (at room temperature). Leibovitz culture medium L-15 (Sigma), 0.72 mg ml^{-1}, was added to improve the viability of the retina (see Koskelainen *et al.* 1994). Sodium-L-aspartate (2 or 4 mM) was added to block synaptic transmission to second-order neurones. In addition, $BaCl_2$ (10 mM) was added in the lower electrode space, from where it would slowly diffuse through the retina to suppress glial currents by blocking potassium channels located mainly at the endfeet of Müller cells (Bolnick *et al.* 1979; Donner & Hemilä, 1985; Newman, 1989). The temperature was controlled by a heat exchanger below the specimen holder and monitored with a thermistor in the bath close to the retina (Ala-Laurila *et al.* 2002).

Toad experiments. Common toads (*Bufo bufo*) were caught in the wild in September in SW Finland and kept unfed in hibernating conditions (at *ca* 5°C). The animals were dark-adapted for at least 12 h before the experiment, decapitated and double-pithed. The rest of the procedures were as described for the rats, except for the composition of the Ringer solution which was (mM): Na^+ 111.3, K^+ 2.5, Mg^{2+} 1.5, Ca^{2+} 1.0; Cl^- 113.0, glucose, 10.0; EDTA, 0.01; Hepes, 12.0.

Recording and light stimulation. The transretinal potential was recorded with two Ag–AgCl electrodes, one in the space under the retina and the other in chloride solution connected to the perfusion Ringer solution through a porous plug. The DC signal was amplified 10 000 ×, digitized at 200 Hz and stored on a computer hard disk.

Stimulus pulses and steady background lights were provided by a dual-beam optical system (Donner *et al.* 1988). In the rat experiments, the common light source was a 50 W tungsten lamp and the light intensities of the two beams were controlled separately with calibrated neutral density filters and wedges. Both the stimulus and the background channel produced homogeneous full-field illumination. Stimulus (519 nm) and background (503 nm) wavelengths were produced with interference filters (Melles Griot, half-transmission bandwidth *ca* 10 nm) and stimulus light pulses ('flashes') were provided by a computer-controlled Compur shutter. In the toad experiments the stimulus light was provided by a 543.5 nm

He–Ne laser (Melles Griot 05 LGR 173, 0.8 mW). In both cases, the duration of the flash was 20 ms.

Calibration of light intensities in terms of photoisomerization rates in rods

The absolute intensity of the unattenuated beam (photons mm^{-2} s^{-1} incident on the retina) in both channels was measured in each experiment with a calibrated photodiode (EG & G HUV-1000B; calibration by the National Standards Laboratory of Finland). Conversion into photoisomerizations per rod per second (Rh^* s^{-1}) requires knowledge of rod dimensions and rhodopsin density. For *Bufo bufo* of the same population as used here, Aho *et al.* (1993) concluded that 34% of incident 525 nm photons (the wavelength they used) cause isomerizations in toad rods. Recalculated to the wavelength of maximum absorbance λ_{max} (501.4 nm) according to the Govardovskii *et al.* (2000) template this corresponds to 40%. For rat, however, values from older literature must be viewed with caution due to technical limitations and possible differences between strains and, e.g. rearing light regimes (see Reiser *et al.* 1996). We therefore decided to measure the crucial parameters directly in the rat strain used for the present experiments.

The widths of rod OSs measured in transverse sections of fixated, eosin-stained rat retina ranged from 1.5 to 2.0 μm with a median value of 1.7 μm. In freshly isolated, torn retina in Ringer solution, the width distribution of all OSs (cell-attached as well as broken-off) was slightly skewed towards higher values, but on the rim of the best-ordered pieces of retina 1.7 μm was the median value for cell-attached OSs. The lengths of the morphologically best-preserved OSs in the fresh preparation ranged from 19 to 26 μm, with 22 μm as a median value. The thickness 1.7 μm is as reported for 'albino rats' by Hagins *et al.* (1970). The length 22 μm is somewhat smaller than the value 24 μm found by Hagins *et al.* (1970), but larger than 20 μm as reported by Mayhew & Astle (1997). Using our median values, we get an OS volume of 50 μm^3. As *Bufo bufo* rod OSs are 45 μm long and 7.4 μm thick (Aho *et al.* 1993), the ratio of rod OS volumes in toad and rat is about 39.

For the specific absorbance of rhodopsin in rat rods, Penn & Hagins (1972) used the value 0.01 μm^{-1}. With progressive improvement of microspectrophotometric (MSP) techniques since the 1960s, however, estimates for many small cells initially thought to have very low absorbance (including human rods and cones) have risen to at least 0.014 μm^{-1} (see, e.g. Dartnall *et al.* 1983), and the value of Penn and Hagins must now be regarded as unrealistically low. We first made new MSP measurements, only to realize (once again) how difficult it is to get reliable measurements of absolute absorbance in such thin OSs. The highest specific absorbances we measured by MSP were around 0.012 μm^{-1}, but we concur with Dr V. I. Govardovskii (personal communication) in regarding this as a lower bound.

We therefore chose an alternative rationale, determining axial absorbance in single rods from whole-retina measurements. The isolated retina was flat-mounted on the bottom of a horizontal glass chamber (76 mm × 26 mm × 5 mm in size) with a clear circular measurement area 3 mm in diameter bordered by a groove 1 mm deep and 2 mm wide. The retina was held in place by a black metal ring (3 mm inner and 9 mm outer diameter), which also served as a mask against light scattered from the groove. The chamber was filled with Ringer solution with 50 mM hydroxylamine added to prevent pigment regeneration. The absorbance due to rhodopsin was determined by comparing the percentage of a dim, 501 nm, 2-s test light pulse transmitted through the retina before and after a 'total bleach', i.e. an exposure estimated to bleach more than 99.7% of the pigment. The test light itself was estimated to bleach only a negligible amount ($< 0.01\%$) of the dark-adapted complement of rhodopsin. The beam was perpendicularly incident from the receptor side, producing a homogeneous field over the exposed retinal area. The measurements were made at room temperature with the calibrated photodiode mentioned above. Values from four retinas were accepted on the basis of the morphological integrity of the OS layer as judged by visual inspection after the measurement. The fraction of the test light absorbed by rhodopsin in the flat-mounted rat retina (mean ± S.E.M.) was 0.502 ± 0.008 ($n = 4$) (or conversely: the mean fraction transmitted was 0.498).

The wavelength (503 nm) we used for background light in the adaptation experiments differs negligibly from the above test wavelength (501 nm), and we may assume that 50% of this light is absorbed. Taking the quantum efficiency for isomerization as 0.67 (Dartnall, 1972), 34% of our background photons produce isomerizations in rat rods. At the wavelength we used for stimulus flashes (519 nm) in the experiments, however, the absorbance of rat rhodopsin has dropped to 89% of its maximum value, and thus only 30% of our 'stimulus' photons produce isomerizations.

As the stimulus light in the ERG experiments and the calibration measurements came from the photoreceptor side of the retina, light-collecting properties of the inner segment can be neglected and the cross-sectional area of rods taken as $\pi\ (1.7/2)^2\ \mu m^2 = 2.27\ \mu m^2$.

Estimates for the specific absorbance of rhodopsin in rat rod OSs may be obtained as follows. If the retina is modelled as a homogeneous absorbing layer 22 μm thick (the length of the OS), specific absorbance becomes $0.0138 \pm 0.0004\ \mu m^{-1}$ (mean ± S.E.M.). Assuming hexagonal packing of photoreceptors and neglecting the

very sparse population of cones, *ca* 90.7% of the retinal cross-sectional area is occupied by rod OSs. Thus the fraction 0.093 of the light passes unattenuated between cells and the fraction transmitted through rod OSs is 0.498–0.093 = 0.405. Specific absorbance then becomes 0.0159 μm^{-1} which is close to the best estimates from amphibians (e.g. *Bufo marinus*, 0.0161 μm^{-1}; Hárosi, 1975) and in fair agreement with a recent estimate of 0.019 μm^{-1} for mouse rhodopsin rods by Nikonov *et al.* (2005) reached by a different method (see Lyubarsky *et al.* 2004).

Experimental protocol

Rod responses to 20 ms flashes were recorded (i) in the dark-adapted state at different temperatures and (ii) at fixed temperature under a series of steady adapting lights of increasing intensities. The temperature and background ranges were 5–36°C and 0–6700 $Rh^* s^{-1}$, respectively.

After dissection, the retina was allowed to adapt in darkness for 1–2 h at 20°C before the experiment was started. First, a few response families to flashes of increasing intensity covering the dynamic range of the rods were recorded at 20°C. These data were later used for anchoring data from different retinas with somewhat different sensitivities to a common reference point. The temperature was then set to a selected value and the retina was left to adapt to the new temperature in darkness for 1–2 h, whereafter a dark-adapted response family was recorded at the new temperature. In 'temperature' experiments, this cycle was repeated at several temperatures. In 'background' experiments, a steady adapting light was turned on without further change of temperature and the rods were allowed to adapt for at least 15 min to ensure that both the fast and slow phases of light adaptation were complete (Calvert *et al.* 2002). At each background intensity, at least three response families were recorded with the same set of stimulus intensities. The background intensity was then increased and the cycle repeated.

Analysis of intensity–response functions

From families of photoresponses to four to six flash intensities, intensity *versus* response amplitude at time-to-peak (*I–R*) data were extracted and fitted with model functions. Data at body temperature were well fitted by an exponentially saturating function (Lamb *et al.* 1981):

$$\frac{R}{R_{\max}} = 1 - e^{-SI} \quad (1)$$

where S is fractional sensitivity, i.e. the fraction of the light-sensitive current turned off per photoisomerization per rod, and $R_{\max}$ is the amplitude of saturated responses. Equation (1) has been successfully applied to rod data from several mammals (monkey, Baylor *et al.* 1984; guinea pig, Matthews, 1991; rat, Robinson *et al.* 1993; human, Kraft *et al.* 1993). At 12°C and lower, a better fit was provided by the shallower Michaelis function:

$$\frac{R}{R_{\max}} = \frac{I}{I + I_{1/2}} \quad (2)$$

where $I_{1/2}$ is the stimulus intensity that elicits a response with half of the saturating amplitude. This function has been used, e.g. for reptilian and amphibian photoreceptors (turtle, Baylor *et al.* 1974; toad, Baylor *et al.* 1979*b*). In the temperature range from 12 to 37°C, there was a smooth transition from Michaelis to exponential saturation behaviour. To get a good fit at all temperatures, we used a weighted sum of the two functions, with a temperature-dependent weighting coefficient $\alpha(T)$ ($0 < \alpha < 1$). The parameters S and $I_{1/2}$ that define the position on the log intensity axis of functions (1) and (2), respectively, are related by $I_{1/2} = 1/S$. The weighted sum is:

$$\frac{R}{R_{\max}} = \alpha(1 - e^{-SI}) + (1 - \alpha)\left(\frac{I}{I + S^{-1}}\right) \quad (3)$$

It is worth noting that the differences between the functions (1), (2) and (3) concern the mid-range of flash intensities. At low stimulus intensities (the linear response range) they all converge and yield the same value of fractional sensitivity S.

The model used for fitting the derived fractional single-quantum response (SQR_f)

To resolve component processes underlying changes in photoresponses, we fitted dim-flash photoresponses with a model for the linear response range by Fain *et al.* (2001), which attempts to include the main reaction steps in the phototransduction cascade in a simple yet realistic manner. It is basically a stripped version of the more detailed model of Nikonov *et al.* (1998, 2000). We chose it mainly because the level of simplification appears suitable for our present purposes, realizing that some other models might have served almost equally well (e.g. Hetling & Pepperberg, 1999; Friedburg *et al.* 2001). The main simplifying assumptions are: (1) the longitudinal diffusion of cGMP and calcium is assumed to be fast enough to provide an instantly 'well-stirred OS' without concentration gradients; (2) changes in intracellular calcium are assumed to follow instantly upon changes in the cGMP-gated current; (3) the only calcium-mediated feedback in the process is the activation of the guanylate cyclase when the calcium concentration declines (see Burns *et al.* 2002).

Because of its neglect of other calcium-mediated feedback effects as well as all saturation effects, the

model is best used for the early phases of dark-adapted, linear-range responses. For this analysis, we fractionalized the responses by dividing the linear-range photoresponses with the saturated response amplitude. Thus we obtained unitless responses that enable comparison between different retinas, animals and recording techniques. Fractional responses per photoisomerization (denoted SQR_f, the average 'fractional single-quantum response') were obtained by scaling the fractional linear-range responses by the flash intensity ([Rh*]).

In the model the change in the fractional photocurrent $r(t)$ at time t due to 1 Rh* is:

$$\frac{dr(t)}{dt} = -(mn_{cG} + 1)\,\beta_{dark} \cdot r(t) + n_{cG}\beta^*(t) \quad (4)$$

Here, m is the co-operativity for the inhibition of guanylate cyclase by Ca^{2+}, n_{cG} is the Hill coefficient of the cGMP-gated channels, β_{dark} is the basal phosphodiesterase activity and $\beta^*(t)$ is the flash-induced phosphodiesterase activity. For our low flash intensities, we use the expression for $\beta(t)$ derived by Lyubarsky & Pugh (1996):

$$\beta^*(t) = \Phi\nu_{RE}\beta_{sub}\frac{\tau_R\tau_E}{\tau_R - \tau_E} \times \left(\exp\left(-\frac{t - t_d}{\tau_R}\right) - \exp\left(-\frac{t - t_d}{\tau_E}\right)\right) \quad (5)$$

where Φ is flash intensity in numbers of photoisomerizations per rod (Rh*], ν_{RE} is the rate of formation of active phosphodiesterase subunits (E*) due to one molecule of photoactivated rhodopsin (R*), β_{sub} is the rate of cGMP hydrolysis due to one E* and τ_R and τ_E are the average lifetimes of R* and E*, respectively.

Equations (4) and (5) were combined and solved numerically by Newton's method. The expression $r(t)$ was fitted to the derived fractional single-quantum response (SQR_f). Three main response-shaping parameters: $\nu_{RE}\beta_{sub}$ for the activation rate, τ_R as a deactivation time constant and β_{dark} for background PDE activity, plus a fourth parameter t_d for the initial response delay, were adjusted for optimal fit by a least-square criterion. The second deactivation time constant τ_E was constrained to have a constant relation to τ_R. (As τ_R and τ_E appear symmetrically in eqn. (5) they cannot be teased apart by curve-fitting.) The stretch of response used for fitting varied somewhat depending on the point where a second, slower recovery component became dominant (Burns *et al.* 2002; Zhang *et al.* 2003; see Fig. 5 below).

Results

Recording rod responses by ERG across the rat retina: removal of glial currents by barium

The transretinal ERG voltage reflects changes in all radial currents in the retina. Even when synaptic transmission to second-order neurones has been blocked by aspartate, the ERG signal contains a strong component due to glial (Müller cell) currents evoked by light-dependent changes in the potassium concentration around photoreceptors (Tomita & Yanagida, 1981). In amphibians this component ('the slow PIII') can be successfully eliminated by perfusion with barium-containing Ringer solution, uncovering rod photoresponses that are very similar to current photoresponses of single cells (Bolnick *et al.* 1979; Donner & Hemilä, 1985). Barium acts by blocking potassium channels located primarily in the vitreal endfeet of Müller cells (Newman, 1989). When testing barium for this purpose in rat retina, we therefore added it (10 mM $BaCl_2$) only to the Ringer solution filling the lower electrode space of the specimen holder, adjacent to the inner retina. We reasoned that this would minimize possible side-effects of Ba^{2+} on the rods themselves, while still allowing sufficient diffusion to Müller cells.

The shapes of flash responses suggested that we did achieve efficient suppression of Müller-cell currents in this way, as illustrated in Fig. 1. With no barium added (panel *A*), ERG flash responses carry a late 'dome' never seen in responses from single rods. This component becomes very large at high flash intensities. By contrast, the responses recorded with Ba^{2+} present in the lower electrode space (panel *B*) are similar to current responses recorded in single mammalian rods (Baylor *et al.* 1984; Burns *et al.* 2002; see Fig. 2 below). Particularly, the presence of an extended, virtually horizontal plateau in the saturated responses suggests that the glial component is now absent or at least negligible.

General characteristics of dark-adapted photoresponses at different temperatures

Figure 2 illustrates the general features of dark-adapted rod photoresponses recorded at two temperatures. Panels *A* and *B* show families of averaged responses to five sets of flashes covering an approximate 3 log unit intensity range (from 1.5 to 2300 Rh* in Fig. 2*A* and from 9.2 to 2300 Rh* in Fig. 2*B*), recorded at 12 and 28°C in the same retina. The dim-flash responses were well fitted by phenomenological models commonly used to describe responses of single rods, such as the 'independent activation' model of Baylor *et al.* (1974, 1979*a*) with the number of stages $n = 4$ (Fig. 2*C*). In the responses to the strongest flashes, however, a transient 'nose' component is seen. It is likely to be of multiple origin, including cone currents as well as currents from voltage-sensitive channels in the rod inner segment (see Green & Kapousta-Bruneau, 1999). In dim-flash responses of rods, which mainly concern us here, such components will be negligible. The amplitude of the saturated rod response (R_{max}), which is needed for calculation of fractional sensitivities, can be read in a consistent manner from the response plateau following

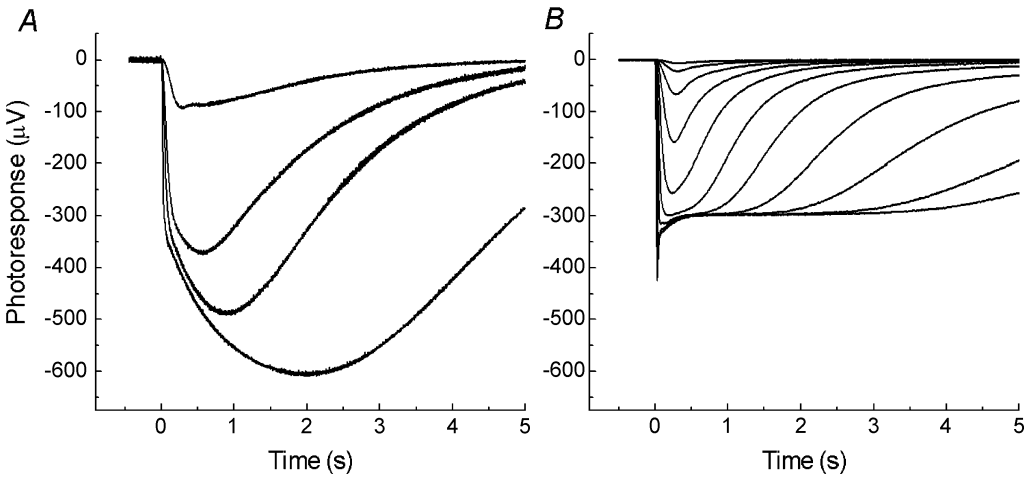

Figure 1. Barium suppresses the glial component of ERG photoresponses from rat retina
A, responses to brief flashes of light recorded at 25°C without barium. Flash intensities: 5, 50, 150 and 1500 Rh*. *B*, responses to brief flashes of light recorded at 28°C with 10 mM $BaCl_2$ in the Ringer solution filling the lower electrode space. The intensity of the strongest flash is 40 000 Rh*; the other flashes go from 0.5 to 15000 Rh* in 0.5 log unit steps.

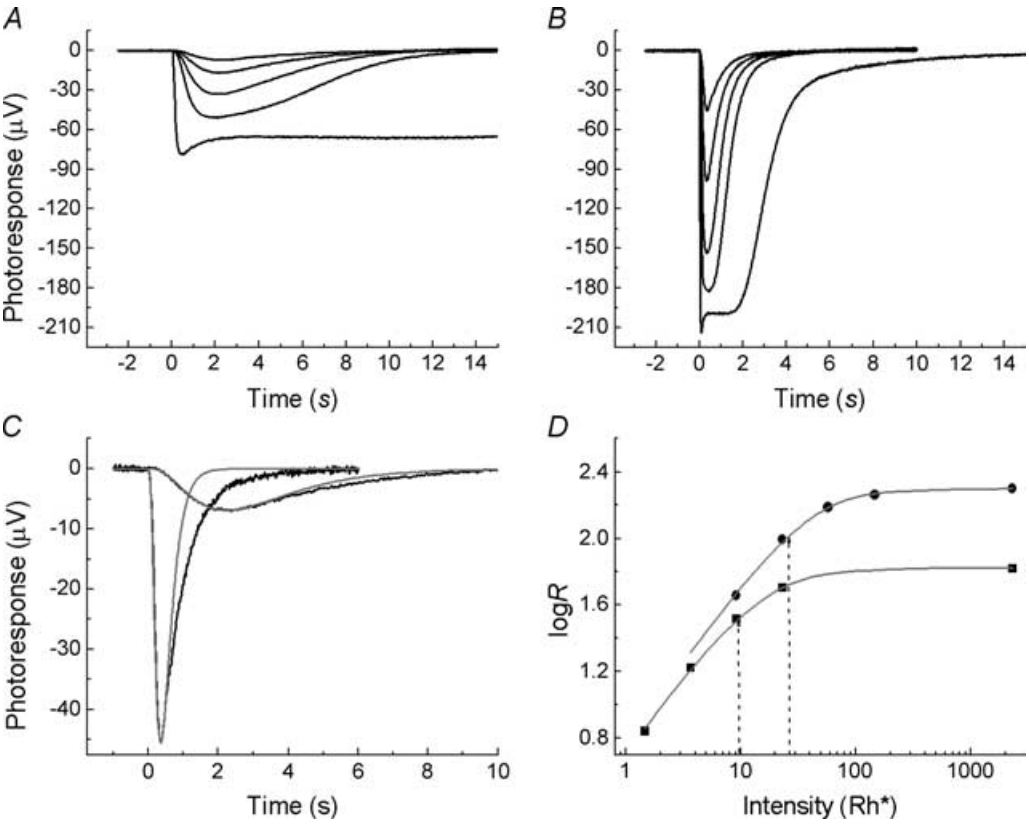

Figure 2. Flash responses and intensity–response functions of rat rods at two temperatures
A and *B*, response families to brief flashes of light recorded in one rat retina at 12°C (*A*) and 28°C (*B*). Flash intensities in *A*: 1.5, 3.7, 9.2, 23 and 2300 Rh*; in *B*: 9.2, 23, 58, 146 and 2300 Rh*. *C*, comparison of the smallest (linear-range) responses from *A* and *B*. The grey curves fitted to the responses trace the 'independent activation' model of Baylor *et al.* (1974) with the number of stages $n = 4$. *D*, intensity–response (*I–R*) functions extracted from the flash responses shown in *A* and *B*. The smooth curves are weighted sums of Michaelis and exponential saturation functions (eqn (3)). The dashed lines indicate the points where the respective *I–R* function has risen halfway to the saturation plateau. See text for further details.

the decay of the nose, although this may yield a slight underestimate.

Raising temperature from 12 to 28°C increased R_{max} from 66 to 200 μV, reflecting an increase in the circulating current (see Lamb, 1984; Donner *et al.* 1988; Robinson *et al.* 1993). Dim-flash responses grew relatively less, implying that S decreased. Warming also compressed the time scale of responses. The time to peak (t_p) of linear-range responses in this retina decreased from 2.2 s at 12°C to 0.36 s at 28°C. The decreases in size and duration of the SQR_f will both contribute to shortening the time spent in saturation in the response to the strongest (2300 Rh*) flash, from 15 s or more in Fig. 2*A* to less than 2 s in Fig. 2*B*.

Figure 2*D* shows the respective intensity–response (*I–R*) functions (squares for 12°C, circles for 28°C). The data were fitted in logarithmic form with a linear combination of Michaelis and exponential saturation functions (eqn (3)), the optimal weight parameter α being 0.46 at 12°C and 0.32 at 28°C. The fractional sensitivities S were 0.084 and 0.025, respectively. Graphically, the lower S at the higher temperature is evident as a rightward shift (i.e. towards higher log I) of the point where the *I–R* function has risen halfway to the saturation plateau (indicated by a dashed line in Fig. 2*D*).

Temperature dependence of fractional sensitivity in darkness

Dark-adapted fractional sensitivities measured in a total of 20 rat retinas are shown as a scatter diagram in Fig. 3*A*. In Fig. 3*B*, the mean values at each temperature are plotted as filled circles. In the range 12–36°C, mean fractional sensitivity in darkness (S_{dark}) (± S.E.M.) decreased monotonically with warming, from 0.085 ± 0.05 Rh^{*-1} ($n = 9$) at 12°C to 0.017 ± 0.002 Rh^{*-1} ($n = 4$) at 36°C. Thus, at body temperature one photoisomerization turned off *ca* 2% of the light-sensitive current, consistent with results from other mammalian species (Baylor *et al.* 1984; Kraft *et al.* 1993), but as much as 8.5% at 12°C. In four retinas, where we obtained sufficiently reliable recordings at 5°C, S_{dark} was 0.096 ± 0.03 Rh^{*-1}, roughly the same as at 12°C, suggesting that this may be a maximal value. One experiment, where the temperature range was sampled at 2–4°C intervals (data plotted as crosses in Fig. 3*A*), indicated that the steady level was reached at *ca* 14°C.

The open circles in Fig. 3*B* show the mean values of fractional sensitivities of rods in three toad retinas. The general trend is similar in rat and toad but the rat function as a whole lies *ca* 0.7 log units above the toad function. We will argue that this can be attributed to the size difference between mammalian and amphibian rod OSs (see further below).

Temperature dependence of photoresponse kinetics in darkness

Figure 4*A* shows the rat rod SQR_f at four temperatures (36, 28, 20 and 12°C) obtained by normalizing dim-flash photoresponses by R_{max} and flash intensity [Rh*]. In Fig. 4*B*, the times to peak (t_p) from experiments on 19 retinas are plotted as filled circles on Arrhenius coordinates (log t_p against T^{-1}). Between 36 and 5°C, mean t_p increased by *ca* 60-fold, from 0.15 ± 0.01 s ($n = 5$) to 9.3 ± 0.3 s ($n = 4$). The change was shallower at the warm end, getting steeper towards lower temperatures, and cannot be well described by a single Q_{10} value over the whole interval. Over the highest 10° (26–36°C), Q_{10} is 2.6, growing to 4.1 in the mid-range (16–26°C) and to 5.4 in the coldest 10° interval (6–16°C).

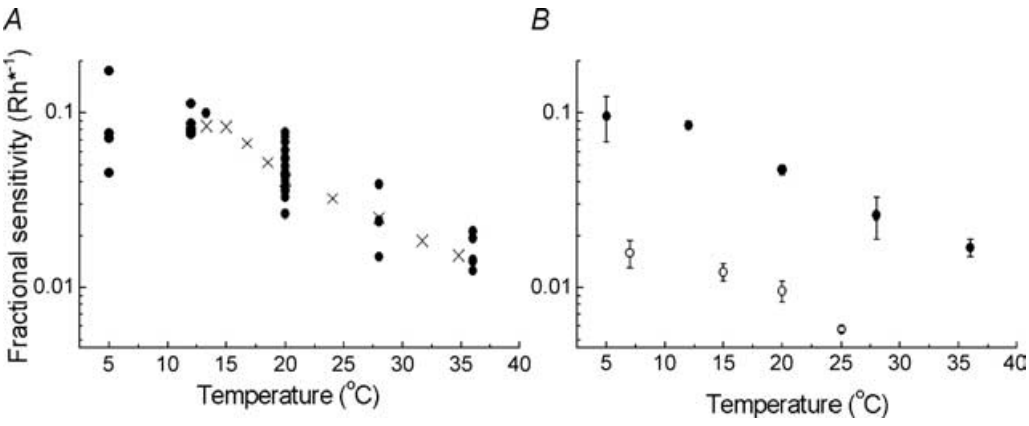

Figure 3. Decrease of fractional sensitivity with rising temperature in rat and toad rods
A, fractional sensitivities (S) of rat rods recorded in 20 retinas at different temperatures. The crosses all refer to a single retina, where S was probed at denser intervals than usual in order to determine with greater precision the temperature where the dependence of fractional sensitivity on temperature levels off. *B*, ●: means (± S.E.M.) of the rat values shown in *A*. ○: means (± S.E.M.) of the fractional sensitivities of rods in 3 toad retinas.

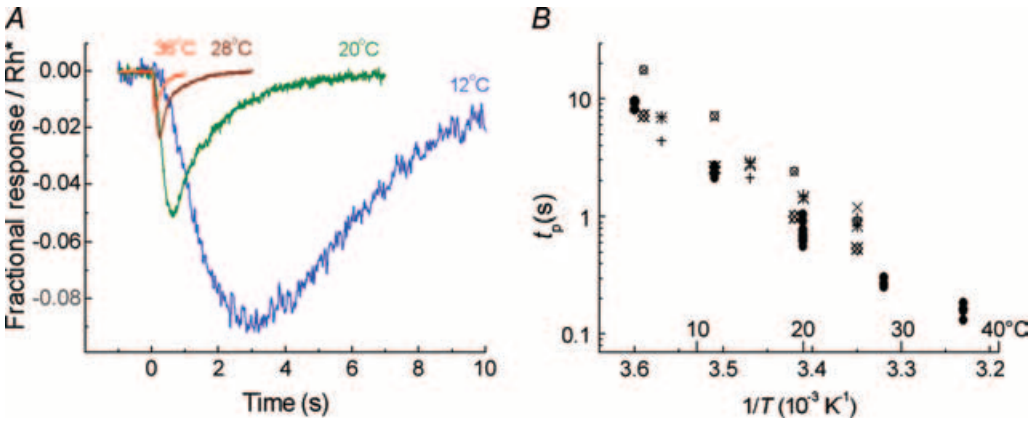

Figure 4. Response acceleration with rising temperature in rat and toad rods
A, fractional responses per unit intensity (SQR_fs) recorded in three different retinas at the temperatures indicated. *B*, times to peak of the SQR_f as function of temperature. ●: rat (experiments on 19 retinas); other symbols: toad (each symbol type refers to one retina).

Toad rod t_p values from experiments on five retinas are plotted by different symbols in the same figure. The overall temperature dependence can be described by a Q_{10} of 3–4. Although the absolute values are slightly higher on average than those of rat, the most striking observation on the whole is how closely t_p of mammalian and amphibian rods agree when referred to the same temperature.

Modelling temperature-dependent changes in the dark-adapted SQR_f

In the temperature range from 36°C to *ca* 20°C, where the change of t_p in rat rods was least steep, SQR_fs could be superimposed by simple scaling of the amplitude and time axis (Fig. 5*A*). The whole response is accelerated or decelerated while retaining its shape, indicating that activation and deactivation processes scale equally with temperature. This agrees with results from amphibian rods (Baylor *et al.* 1983; Lamb, 1984). By contrast, the steeper increase in t_p seen upon strong cooling (5–12°C) was associated with excessive retardation of the recovery phase compared with the activation phase (see Robinson *et al.* 1993). 'Cold' responses could no longer be made to superimpose with 'warm' responses by scaling of the time axis (Fig. 5*B*).

Next, we broke down response kinetics into activation and inactivation components by applying the model summarized by eqns (4) and (5). We use the model

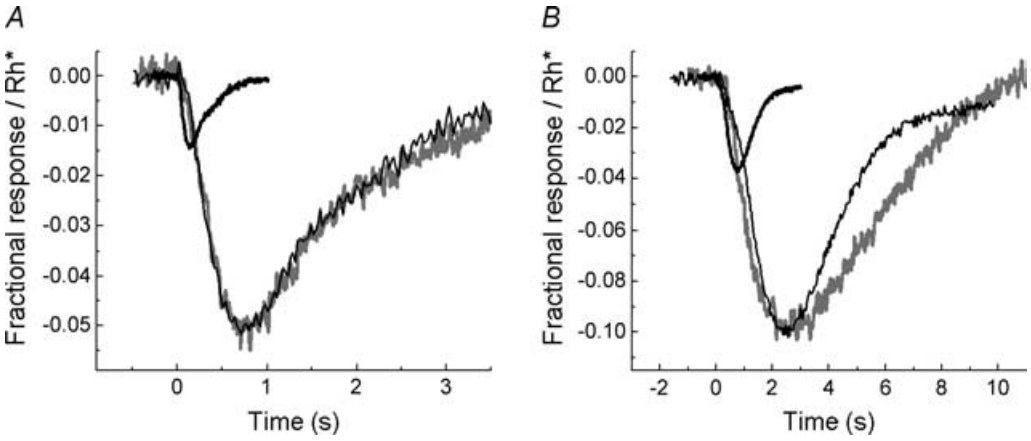

Figure 5. Shape-preserving and shape-changing response deceleration in rat rods
Deceleration of rat rod photoresponses when temperature is lowered from 36°C occurs as if by simple scaling of the amplitude and time axis under moderate cooling (*A*), but includes a change of the waveform under strong cooling (*B*). Shown are SQR_fs recorded at 36°C (black bold trace) and 20°C (grey trace) in *A*, and at 20°C (black bold trace) and 12°C (grey trace) in *B*. In both panels, the black thin trace shows the 'warm' response normalized to the same amplitude and time to peak as the 'cold' response. In each panel, both responses are from the same retina.

Table 1. Model parameters

Parameter name	Unit	Parameter value at: 5°C	12°C	20°C	28°C	36°C
$\nu_{RE}\beta_{sub}$	s^{-2}	0.013 ± 0.005	0.11 ± 0.02	0.72 ± 0.2	2.5 ± 0.5	5.2 ± 2
β_{dark}	s^{-1}	0.06 ± 0.03	0.27 ± 0.06	0.62 ± 0.03	1.44 ± 0.07	2.5 ± 0.4
τ_R	s	3 ± 1	0.76 ± 0.09	0.17 ± 0.007	0.067 ± 0.004	0.037 ± 0.005
τ_E	s	Fixed at $3.75 \times \tau_R$				
n_{cG}	—	Fixed at 2.5				
m_{Ca}	—	Fixed at 2.0				
t_d	s	200 ± 200	140 ± 10	87 ± 10	38 ± 7	18 ± 4

Model parameters (eqns (4)-(5)) that provide best fits to the SQR_f of rat rods at different temperatures. For the identity of the parameters, see text.

primarily as a tool to parametrise different aspects of the SQR_f, realizing that correspondences between the parameters and putative biochemical counterparts must be viewed with caution. At best, we achieve a simple description *consistent* with known phototransduction processes.

Fitting of the model entailed adjustment of four parameters, of which (i) – (iii) are the main determinants of response shape (see Methods): (i) the amplification of the activation process, $\nu_{RE}\beta_{sub}$, (ii) the steady-state phosphodiesterase (PDE) activity in darkness, β_{dark}, and (iii) a deactivation time constant. As the average lifetimes of active rhodopsin (R^*) and phosphodiesterase (E^*), τ_R and τ_E in eqn (5), cannot be teased apart, they were fused into one parameter by locking the ratio τ_E/τ_R as 3.75 (Nikonov *et al.* 2000). This implies that both are assumed to have the same temperature dependence, here captured by τ_R. We tested different values for the τ_E/τ_R ratio (in the range 2.6–4.5) and found that the values obtained for the other parameters were not very sensitive to this ratio. Fitting further involved adjustment of (iv) the delay from the flash to the onset of the response, t_d, in eqn (5). The Hill coefficients for activation of the cGMP-gated channel and for the calcium dependence of the guanylate cyclase were fixed at 2.5 and 2, respectively.

Figure 6 illustrates the quality of the model fits to dark-adapted SQR_fs determined at 20 and 36°C. The parameter values (means ± S.E.M.) obtained at each temperature are summarized in Table 1. Generally, good fits could be achieved at all temperatures, but the variation between experiments in the parameter values was considerable especially at the extreme temperatures (36 and 5°C, see the S.E.M.s in Table 1). The values were mostly consistent with published values for their putative biochemical counterparts in other species (see Discussion).

In Fig. 7, the parameter values for rat rods from Table 1 (filled symbols) are plotted together with corresponding values extracted from our toad experiments (open symbols). In a first approximation, parameters (ii) – (iv) (in Fig. 7*B–D*) behave very similarly in rat and toad, and the only major difference is in the activation parameter (i), shown in Fig. 7*A*. In the Discussion, we will argue that this difference can be explained by the difference in OS size.

Light adaptation at different temperatures

Background adaptation in rat rods was studied at each of the temperatures 12, 20, 28 and 36°C. Figure 8*A* shows the effect of steady adapting light of different intensities on responses to a fixed stimulus intensity in the linear range at 20°C. The figure displays the classic hallmarks of light adaptation, desensitization coupled to response acceleration (e.g. Fuortes & Hodgkin, 1964; Baylor & Hodgkin, 1974), as responses appear to peel off from a common rising edge at earlier times the stronger the background light (e.g. Thomas & Lamb, 1999; Friedburg *et al.* 2001). Figure 8*B* shows (on log–log coordinates) the changes of S with background intensity at different temperatures. Variation in dark-adapted S between individual retinas was corrected for by normalization of

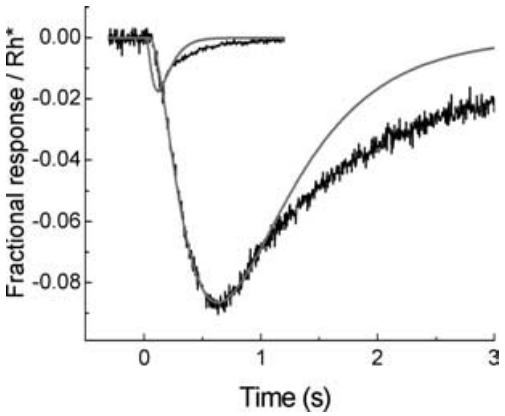

Figure 6. Examples of model fits to rat rod responses
The black noisy traces are experimental SQR_fs from one retina at 20 and 36°C; the grey smooth curves are best fits of the model summarized in eqns (4)–(5).

the data according to the value at the reference temperature 20°C, which was determined in every experiment (see Methods). These differences in S_{dark} were treated as a measure of variation in the light intensity effectively 'seen' by the retinas, and thus the same normalization was applied both along the log stimulus intensity and the log background intensity axis.

As might be expected from the temperature dependence of 'dark' sensitivity, the desensitizing effect of a background light also set in at lower intensities the lower the temperature. The background intensity where S had fallen by 10-fold was denoted I_{10} and taken as an index of the capacity for light adaptation. Mean I_{10} (± S.E.M.) increased strongly with temperature, being 46 ± 2 Rh* s^{-1} ($n = 3$) at 12°C and 4500 ± 500 Rh* s^{-1} ($n = 3$) at 36°C. The parameters of light adaptation in rat rods at different temperatures are summarized in Table 2.

In earlier work, desensitization by background light has often been considered in terms of flash sensitivities (S_{flash} = response amplitude per Rh* for linear-range responses) and it may be difficult or impossible to extract changes in fractional sensitivity S from the data given in the published articles. To facilitate comparison with earlier literature, the light-adaptation data at rat body temperature have been plotted in Fig. 8*C* (on log–log coordinates) also as changes in S_{flash} (black squares), together with the changes in S (red circles). This format shows how the stimulus needed to elicit a response of fixed criterion amplitude changes with background intensity, as amplitude changes depend not only on 'true' adaptation but also on response compression as R_{max} decreases. The flash sensitivity function corresponds to threshold-*versus*-background-intensity (TVI) functions as classically measured, e.g. in psychophysics. As seen in Fig. 8*C*, the TVI and the S functions diverge even around background intensities of *ca* 1 Rh* s^{-1}. The background intensity that depressed flash sensitivity by 10-fold at body temperature (Fig. 8*C*) was about 700 Rh* s^{-1}, compared with I_{10} = 4500 Rh* s^{-1} for fractional sensitivity (Table 2). The corresponding difference became smaller, however, at lower temperatures (not shown).

Discussion

Temperature dependence of photoresponse kinetics in darkness

Over a moderate temperature range (*ca* 20–36°C), the flash response waveforms of rat rods recorded at different

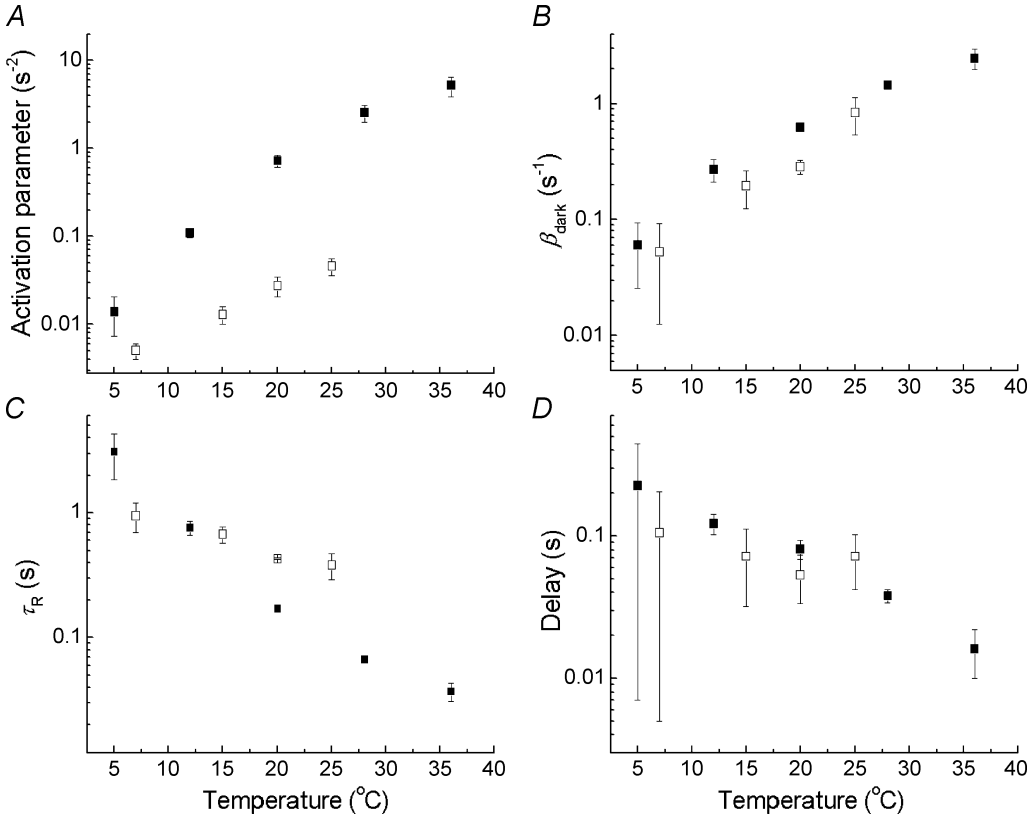

Figure 7. Comparison of the model parameters (mean ± S.E.M.) extracted from rat and toad photoresponses
Filled symbols refer to rat, open symbols to toad. *A*, the activation parameter, $\nu_{RE}\beta_{sub}$; *B*, PDE 'dark' activity, β_{dark}; *C*, inactivation time constant, τ_R; *D*, the photoresponse delay, t_d.

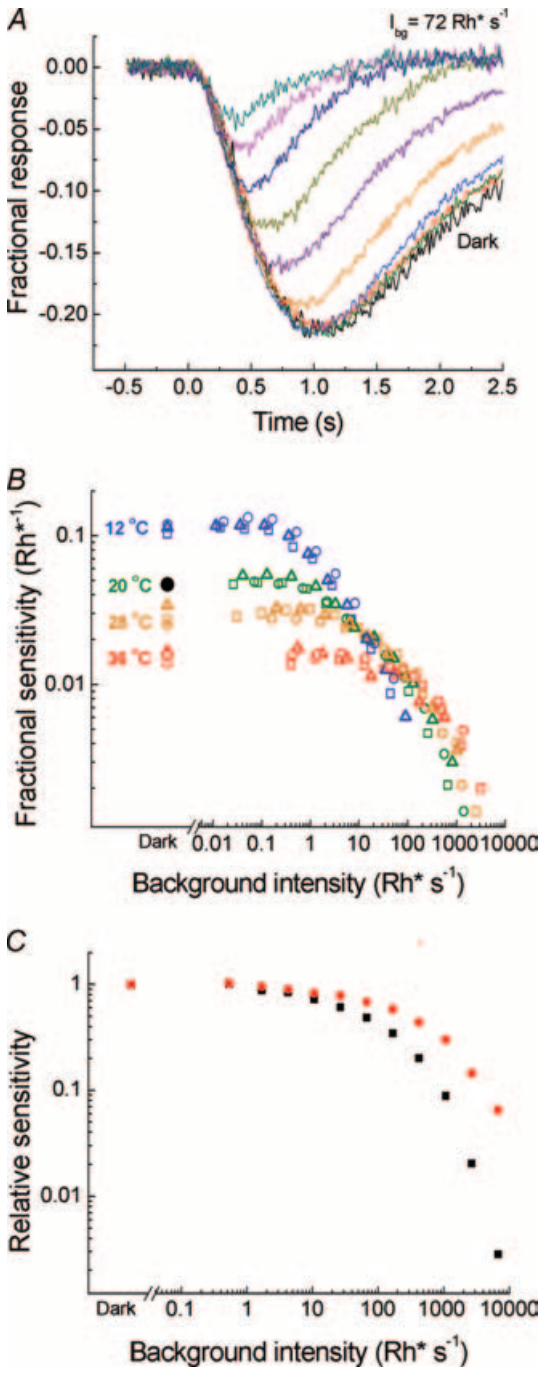

Figure 8. The effect of steady background light on the sensitivity and kinetics of rat rod photoresponses
A, changes of the response (fractional) to a linear-range flash of fixed intensity with increasing intensity of a steady background light at 20°C. The largest response was recorded in darkness; background intensity increases from 0.018 Rh* s^{-1} (response confluent with the dark-adapted response) up to 72 Rh* s^{-1} (smallest response) first in 0.5 log unit steps (up to the first response differing markedly from the dark-adapted response) and then in 0.4 log unit steps. *B*, background adaptation: fractional sensitivity *versus* background intensity at 12, 20, 28 and 36°C. At each temperature, each symbol type refers to an experiment on one retina. In each experiment, a dark-adapted reference fractional sensitivity was determined at 20°C, and the position of the data was normalized according to this common reference (filled black circle) as described in the text. *C*, comparison of fractional sensitivity (red circles) and flash sensitivity (black squares) at rat body temperature on one retina. Both sets of data have been normalized to unity in the dark-adapted state.

temperatures (normalized to equal amplitude) could be superimposed by simple scaling of the time axis. As previously described in amphibians (Baylor *et al.* 1983; Lamb, 1984), the whole response was accelerated or decelerated while retaining its shape, indicating that activation and deactivation processes were affected equally by temperature. In this range, changes in t_p could be described by similar, moderate Q_{10} values (2–4) in both rat and in several species of amphibians (*Bufo bufo*: Fig. 4*B*; *Bufo marinus*: Baylor *et al.* 1983; Lamb, 1984; *Rana temporaria*: Donner *et al.* 1988). By contrast, the steeper increase in t_p seen upon stronger cooling (5–12°C) was associated with excessive retardation of the recovery phase compared with the activation phase, so the basic shape and not only the general time scale of 'cold' and 'warm' responses differed. Obviously, these are temperatures that a living rat can never experience (as opposed to a living frog) and from a functional viewpoint, a breakdown of this aspect of visual constancy in rat is not surprising. From a molecular viewpoint, the implication is that different mechanisms for response shut-off become rate limiting at the lowest temperatures.

The strong retardation of response recovery at low temperatures is in qualitative agreement with observations by Robinson *et al.* (1993) in suction-pipette recordings from single rat rods. In their experiments, however, the effect was much more extreme and covered a wider temperature range. This might indicate dysfunction of the isolated rods in regard to some of the mechanisms for response recovery, which would also explain their very large SQR_fs (0.19 at room temperature and 0.10 at body temperature). Cells drawn into suction pipettes are particularly susceptible to modifications of shut-off and adaptation reactions, whether 'unexplained' (see, e.g. the unnaturally large and slow quantal responses in Baylor *et al.* 1980) or dependent on some identified factor, such as pH buffering (Lamb, 1984; Donner *et al.* 1990*b*). Light adaptation is also easily impaired (Baylor *et al.* 1984; Donner *et al.* 1990*a*). Cells embedded in retinal tissue are likely to be closer to natural functioning.

Modelling of dark-adapted photoresponses: temperature dependence and identity of the activation parameters

The values obtained for the activation parameter $\nu_{RE}\beta_{sub}$ grew steadily with increasing temperature, from

Table 2. Parameters of adaptation to steady background light of rat rods at different temperatures

T (°C)	t_p (s)	S (Rh^{*-1})	I_{10} (Rh* s^{-1})	$I_{10,flash}$ (Rh* s^{-1})	$I_{1/2,flash}$ (Rh* s^{-1})
5	9.3 ± 0.3 (n = 4)	0.096 ± 0.03 (n = 4)	—	—	—
12	2.4 ± 0.06 (n = 9)	0.085 ± 0.05 (n = 9)	46 ± 2 (n = 3)	14 ± 1 (n = 3)	1.6 ± 0.1 (n = 3)
20	0.71 ± 0.03 (n = 20)	0.047 ± 0.003 (n = 20)	300 ± 80 (n = 3)	99 ± 20 (n = 3)	4.5 ± 0.4 (n = 3)
28	0.28 ± 0.01 (n = 3)	0.026 ± 0.007 (n = 3)	1500 ± 400 (n = 3)	370 ± 200 (n = 3)	41 ± 20 (n = 3)
36	0.15 ± 0.01 (n = 5)	0.017 ± 0.002 (n = 4)	4500 ± 500 (n = 3)	700 ± 90 (n = 4)	55 ± 7 (n = 4)

The columns are: t_p, dark-adapted time to peak; S, dark-adapted fractional sensitivity; I_{10}, background light intensity needed to decrease fractional sensitivity by a factor of 10; $I_{10,flash}$, background light intensity needed to decrease flash sensitivity by a factor of 10; $I_{1/2,flash}$, background light intensity needed to decrease flash sensitivity by half. All values are ± S.E.M.

(mean ± S.E.M.) 0.013 ± 0.005 s^{-2} at 5°C, to 5.2 ± 1.5 s^{-2} at 36°C (Table 1). In the range 12–28°C, the temperature dependence of $\nu_{RE}\beta_{sub}$ was described with a Q_{10} of *ca* 7.4. This value is too high for any single biochemical reaction, but not inconsistent with the temperature dependence of two (or more) cascaded stages that accelerate independently with warming, e.g. the rate of PDE activation by R* (ν_{RE}) and the catalytic activity of E* (β_{sub}).

The slightly differently defined activation parameter of Lamb & Pugh (1992), $A = \nu_{RE}\beta_{sub}n_{cG}$, has been widely used to describe activation in a number of species, including human ERG rod responses. To enable comparison, we have to multiply our parameter by the Hill coefficient of the cGMP-gated channel. Setting $n_{cG} = 2.5$, our comparable activation coefficients would be 1.8 ± 0.5 at 20°C and 13 ± 4 at 36°C. In human rods, Friedburg *et al.* (2001) found A values in the range 3–7 (at body temperature); clearly, our value of 13 is significantly higher. As the waveforms described by both are rather similar, however, the difference must be associated with model formalism, and it is easy to see where it lies. In the model of Lamb & Pugh (1992) and Friedburg *et al.* (2001), the onset of inactivation reactions is subject to a time delay. In that case, a longer stretch of the rising response will be interpreted as an index of pure activation. Our model with instant onset of inactivation reactions produces an early departure from the 'activation-only' curve, and even the rising edge of the recorded response mainly emerges as the result of (steeper) activation counteracted by incipient inactivation.

Activation in rat and toad

Comparison of activation parameters between species requires that differences in OS volume be taken into account. The smaller volume of a rat rod compared with a toad rod implies that the same rate of PDE activation will produce a faster change in cGMP *concentration*, and since it is a change in concentration that modulates the channels, the response per R* will be larger in rat than in toad even if there is no difference in PDE activation. Conversely, this must be observed when PDE activity is derived from measurement of the photoresponse. As shown below, we then find that the deduced rate of PDE activation by R* (ν_{RE}) in our rat rods is similar or even somewhat lower than in toad rods, the much higher fractional sensitivity of rat rods notwithstanding.

In the model, the catalytic activity of E* (β_{sub}) is the parameter that will scale with cytoplasmic volume, being expressed in terms of concentration changes ($\beta_{sub} \propto 1/V_{cyto}$, Lamb & Pugh, 1992). Leskov *et al.* (2000) report $\beta_{sub} = 4.3 \times 10^{-4}$ s^{-1} for toad rods at 22°C. Their rod OSs were *ca* 34 times larger than those of our rats. Taking $\beta_{sub} = 34 \times (4.3 \times 10^{-4}\ s^{-1}) = 1.46 \times 10^{-2}$ s^{-1} for rat rods and interpolating $\nu_{RE}\beta_{sub}$ from Table 1 to room temperature we get $\nu_{RE} \approx 68$ s^{-1}. This is rather close to the value of 76 s^{-1} obtained by Melia *et al.* (1997) by biochemical measurements from bovine rod outer segments at 23°C, but clearly less than the 120 s^{-1} given by Leskov *et al.* (2000) for toad rods. A similar analysis of our own *Bufo bufo* data gives $\nu_{RE} \approx 90$ s^{-1} (whereby a slight difference in OS volume between our toad rods and those of Leskov *et al.* has been taken into account). The estimates obtained this way should be considered as no more than indicative of a presumed 'real biochemical' ν_{RE}, as they are sensitive to the method of interpolation, variations in outer segment size and, most significantly, to the validity of the approximation of the OS as a well-stirred compartment. Alternatively, we might assume, for example, that the longitudinal spread of the quantal activation is always constant around the activated interdiscal space, the width of which does not vary with OS size. The parameter β_{sub} would then scale with the OS cross-sectional area only, yielding $\nu_{RE} \approx 180$ s^{-1} for rat rods. With respect to errors due to uncertainty in the proper scaling by OS size, this estimate (the result of another oversimplification) may be taken as an upper bound.

At any rate, it appears that the 5–7 times higher fractional sensitivity of mammalian rods compared with amphibian rods at any given temperature is achieved with a similar or even lower rate of PDE activation by a single R*. It may be noted, however, that our experimental technique could cause some underestimation of the activation parameter. The ERG signal is a mass response from thousands of rods, and variation between cells might

cause the initial rise of the population response to be shallower than that of a single cell.

Other response parameters

The parameter putatively associated with PDE background activity, β_{dark}, also grew monotonically with temperature, although less steeply, with apparent $Q_{10} = 2.7$ in the range 12–36°C. The value 0.62 s^{-1} at 20°C is well within the range of published estimates of PDE 'dark' activity, while the value for mammalian body temperature (2.5 s^{-1}) is somewhat higher than the estimate 1.2 s^{-1} given by Tamura *et al.* (1991) for primate rods (see also Nikonov *et al.* 2000). Interestingly, our simulations of photoresponses (not shown) indicate that the changes in the PDE background activity parameter β_{dark} alone can explain the desensitizing effect of rising temperature in both our model species. The strong increase of the initial amplification with warming would rather serve to sensitize the photoreceptors, even when partly balanced by the less steep changes in the inactivation time constants.

The 'fused' inactivation time constant τ_R decreased in monotonic but decelerating fashion towards higher temperatures. Mean ± S.E.M. values for τ_R decreased from 3 ± 1 s at 5°C to 0.037 ± 0.005 s at 36°C. The delay parameter t_d also showed a continuous decrease with warming, being 200 ± 200 ms at 5°C and 18 ± 4 ms at 36°C.

On the applicability of the model

While there exists a considerable amount of literature on modelling the phototransduction cascade starting from the activation of a single rhodopsin molecule towards the full photoresponse of the photoreceptor (see Methods), there is as yet no unified model covering all aspects of photoresponses (see Hamer, 2000). The most detailed phototransduction models available deal with amphibian photoreceptors, for which there is most, e.g. biochemical, data available. The model used in this work is a greatly simplified version of models with wider scope. The simplifications suit our purpose of describing the fractional single photon response with a handful of parameters apparently representative of elements of the phototransduction cascade, allowing us to parametrize the temperature dependence of the SQR_f. For a more rigorous study of the rat phototransduction cascade we would immediately have to take into account the time-dependent calcium kinetics including extensive buffering of this ion in the outer segment. This is not well characterized in mammalian photoreceptors and would not aid our qualitative discussion about the change in the rat SQR_f. It should be noted, though, that calcium buffering will especially affect the interpretation of response recovery, and may play a role in the deviation of the responses from the model curve in the later phase of recovery.

Light adaptation

The observed change in the adapting efficiency of steady background light as temperature was raised from 12 to 36°C ($\Delta \log I_{10} = 1.96$) correlates fairly well with changes in the time integral of the fractional photon response. Given that $\Delta \log S = 0.76$ and $\Delta \log t_p = 1.09$ (at I_{10}), the integrated response changes by 1.85 log units over the same temperature range.

The earliest rising edge of the SQR_f remained constant under adapting background lights, as previously observed in several species including humans (Thomas & Lamb, 1999; Friedburg *et al.* 2001). The simplest interpretation is that the activation constant was unaltered by light adaptation.

The desensitization by background light of rat rods at body temperature was similar to that observed in humans by Friedburg *et al.* (2001), the background intensity that depressed flash sensitivity by 10-fold being *ca* 700 $Rh^* s^{-1}$ in the rat retina and 860–1700 $Rh^* s^{-1}$ in the human eye. Most of the desensitization in this range was associated with response compression, however, and it is difficult to compare changes in fractional sensitivity S, which in the experiments of Friedburg *et al.* (2001) covered no more than 0.8 log units (due to technical limitations). While the same difficulty pertains to many other studies of mammalian rod adaptation, changes in flash sensitivity under background light are consistently in fair agreement with ours. For example, Tamura *et al.* (1989) report a response-halving background of 35 $Rh^* s^{-1}$ for cat rods, while our corresponding value from Fig. 8*C* is about 55 $Rh^* s^{-1}$. Other comparable values are 42 $Rh^* s^{-1}$ for rabbit (Nakatani *et al.* 1991*a*), 52 $Rh^* s^{-1}$ for cynomolgus monkey (Nakatani *et al.* 1991*b*) and 120 $Rh^* s^{-1}$ for human (Kraft *et al.* 1993). The main point is that our rat rods at 36°C seem to be fairly representative of mammalian rods in general. Still, they were found to adjust their fractional sensitivity S as efficiently as amphibian rods when studied at similar temperatures. For example, at 12°C I_{10} was about 46 $Rh^* s^{-1}$, compared with *ca* 10 and 80 $Rh^* s^{-1}$ measured in frog rods at, respectively, 9 and 16.5°C (Hemilä, 1977; Donner *et al.* 1995). We conclude that the great difference in adaptation capacity that has been claimed to exist between mammalian and amphibian rods is mainly explained by differences in experimental temperature.

Homeothermy and the size of rod outer segments

Given our conclusion that the phototransduction molecules work remarkably similarly in mammalian and amphibian rods, the major difference is the thickness of the OS. Obviously, the slender rods of mammals are

not an adaptation for visual acuity: as rod signals are always neurally pooled, single rods do not constitute independent image points. Rather, it is instructive to consider the thin OS as an adaptation to a high and stable body temperature. First, it allows generation of big photon responses within the compressed time scale afforded by the high reaction temperature. In mammalian rods the quantal response in the dark-adapted state at body temperature reaches approximately the fraction 0.02 of the saturating response amplitude and peaks at *ca* 200 ms (our Fig. 4; see Baylor *et al.* 1984; Kraft *et al.* 1993; Burns *et al.* 2002). The quantal response of amphibian rods at 15–20°C has about the same fractional amplitude, but peaks at *ca* 1 s (Baylor *et al.* 1979*b*, 1980, 1983; Lamb, 1984; Donner *et al.* 1990*a*). A large quantal response is advantageous, since one prerequisite for maximizing the signal-to-noise ratio of vision in dim light is that the signals generated at the input stage are large enough not to be swamped by noise injected at later stages (synaptic noise, channel noise, etc.). Unfortunately, the noise component that is due to random thermal activation of rhodopsin itself will benefit from the same amplification as the photon-induced signal, and such light-identical thermal noise will be particularly troublesome in a 'warm-blooded' animal (Baylor *et al.* 1984). This points to the second advantage of a thin OS. Packing the noise-producing rhodopsin molecules into many small outer segments rather than few big ones will allow the rod synapse to work at a high gain without undue saturation pressure from thermal photon-like events (true also for quantal noise from dim background light). Achieving the size reduction by narrowing rather than shortening the OS keeps axial photon catch high and diffusional distances from disks to the plasma membrane short. The accompanying increase in surface-to-volume ratio will also speed up the recovery of the cell after a bleaching exposure (Ala-Laurila *et al.* 2005).

It would be misleading, however, to view the fat outer segments of amphibians simply as a 'default' solution, acceptable in the absence of particular opposing selection pressures. There may be clear advantages associated with having thick cells. First, it is energetically economical to have a low surface-to-volume ratio. Second, although rat rod OSs are fairly long in relation to their width, they are still only about half the length of toad OSs. It seems likely that maintenance of a very long rod OS to maximize quantum catch and thus dark-adapted visual sensitivity is facilitated by a certain robustness.

References

Aho AC, Donner K, Helenius S, Larsen LO & Reuter T (1993). Visual performance of the toad (*Bufo bufo*) at low light levels: retinal ganglion cell responses and prey-catching accuracy. *J Comp Physiol A* **172**, 671–682.

Ala-Laurila P, Estevez M, Crouch RK, Wiggert B & Cornwall MC (2005). Production and clearance of all-trans retinol in bleached rods and cones depends on opsin type and photoreceptor morphology. *Invest Ophthalmol Vis Sci* **46**, E-Abstract 3968.

Ala-Laurila P, Saarinen P, Albert R, Koskelainen A & Donner K (2002). Temperature effects on spectral properties of red and green rods in toad retina. *Vis Neurosci* **19**, 785–792.

Arshavsky VY, Lamb TD & Pugh EN Jr (2002). G proteins and phototransduction. *Annu Rev Physiol* **64**, 153–187.

Baylor DA & Hodgkin AL (1974). Changes in time scale and sensitivity in turtle photoreceptors. *J Physiol* **242**, 729–758.

Baylor DA, Hodgkin AL & Lamb TD (1974). The electrical response of turtle cones to flashes and steps of light. *J Physiol* **242**, 685–727.

Baylor DA, Lamb TD & Yau KW (1979*a*). The membrane current of single rod outer segments. *J Physiol* **288**, 289–611.

Baylor DA, Lamb TD & Yau KW (1979*b*). Responses of retinal rods to single photons. *J Physiol* **288**, 613–634.

Baylor DA, Matthews G & Yau KW (1980). Two components of electrical dark noise in toad retinal rod outer segments. *J Physiol* **309**, 591–621.

Baylor DA, Matthews G & Yau KW (1983). Temperature effects on the membrane current of retinal rods of the toad. *J Physiol* **337**, 723–734.

Baylor DA, Nunn BJ & Schnapf JL (1984). The photocurrent, noise and spectral sensitivity of rods of the monkey *Macaca fascicularis*. *J Physiol* **357**, 575–607.

Bolnick DA, Walter AE & Sillman AJ (1979). Barium suppresses slow PIII in perfused bullfrog retina. *Vision Res* **19**, 1117–1119.

Burns ME, Mendez A, Chen J & Baylor DA (2002). Dynamics of cyclic GMP synthesis in retinal rods. *Neuron* **36**, 81–91.

Calvert PD, Govardovskii VI, Arshavsky VY & Makino CL (2002). Two temporal phases of light adaptation in retinal rods. *J General Physiol* **119**, 129–145.

Dartnall HJ (1972). Visual pigment of the coelacanth. *Nature* **239**, 341–342.

Dartnall HJA, Bowmaker JK & Mollon JD (1983). Human visual pigments: microspectrophotometric results from the eyes of seven persons. *Proc R Soc Lond B Biol Sci* **220**, 115–130.

Donner K, Copenhagen DR & Reuter T (1990*a*). Weber and noise adaptation in the retina of the toad *Bufo marinus*. *J General Physiol* **95**, 733–753.

Donner K & Hemilä S (1985). Rhodopsin phosphorylation inhibited by adenosine in frog rods: lack of effects on excitation. *Comp Biochem Physiol A* **81**, 431–439.

Donner K, Hemilä S, Kalamkarov G, Koskelainen A & Shevchenko T (1990*b*). Rod phototransduction modulated by bicarbonate in the frog retina: roles of carbonic anhydrase and bicarbonate exchange. *J Physiol* **426**, 297–316.

Donner K, Hemilä S & Koskelainen A (1988). Temperature-dependence of rod photoresponses from the aspartate-treated retina of the frog (Rana temporaria). *Acta Physiol Scand* **134**, 535–541.

Donner K, Koskelainen A, Djupsund K & Hemilä S (1995). Changes in retinal time scale under background light: observations on rods and ganglion cells in the frog retina. *Vision Res* **35**, 2255–2266.

Fain GL (1976). Sensitivity of toad rods: dependence on wave-length and background illumination. *J Physiol* **261**, 71–101.

Fain GL, Matthews HR, Cornwall MC & Koutalos Y (2001). Adaptation in vertebrate photoreceptors. *Physiol Rev* **81**, 117–151.

Friedburg C, Thomas MM & Lamb TD (2001). Time course of the flash response of dark- and light-adapted human rod photoreceptors derived from the electroretinogram. *J Physiol* **534**, 217–242.

Fuortes MGF & Hodgkin AL (1964). Changes in time scale and sensitivity in the ommatidia of *Limulus*. *J Physiol* **172**, 239–263.

Govardovskii VI, Fyhrquist N, Reuter T, Kuzmin DG & Donner K (2000). In search of the visual pigment template. *Vis Neurosci* **17**, 509–528.

Green DG & Kapousta-Bruneau NV (1999). A dissection of the electroretinogram from the isolated rat retina with microelectrodes and drugs. *Vis Neurosci* **16**, 727–741.

Hagins WA, Penn RD & Yoshikami S (1970). Dark current and photocurrent in retinal rods. *Biophys J* **10**, 380–412.

Hamer RD (2000). Computational analysis of vertebrate phototransduction: combined quantitative and qualitative modeling of dark- and light-adapted responses in amphibian rods. *Vis Neurosci* **17**, 679–699.

Hárosi F (1975). Absorption spectra and linear dichroism of some amphibian photoreceptors. *J General Physiol* **66**, 357–382.

Hemilä S (1977). Background adaptation in the rods of the frog's retina. *J Physiol* **265**, 721–741.

Hetling JR & Pepperberg DR (1999). Sensitivity and kinetics of mouse rod flash responses determined *in vivo* from paired-flash electroretinograms. *J Physiol* **516**, 593–609.

Hood DC & Birch DG (1993). Light adaptation of human rod receptors: the leading edge of the human a-wave and models of rod receptor activity. *Vision Res* **33**, 1605–1618.

Koskelainen A, Donner K, Kalamkarov G & Hemilä S (1994). Changes in the light-sensitive current of salamander rods upon manipulation of putative pH-regulating mechanisms in the inner and outer segment. *Vision Res* **34**, 983–994.

Kraft TW, Schneeweis DM & Schnapf JL (1993). Visual transduction in human rod photoreceptors. *J Physiol* **464**, 747–765.

Lamb TD (1984). Effects of temperature changes on toad rod photocurrents. *J Physiol* **346**, 557–578.

Lamb TD, McNaughton PA & Yau KW (1981). Spatial spread of activation and background desensitization in toad rod outer segments. *J Physiol* **319**, 463–496.

Lamb TD & Pugh EN Jr (1992). A quantitative account of the activation steps involved in phototransduction in amphibian photoreceptors. *J Physiol* **449**, 719–758.

Leskov IB, Klenchin VA, Handy JW, Whitlock GG, Govardovskii VI, Bownds MD, Lamb TD, Pugh EN Jr & Arshavsky VY (2000). The gain of rod phototransduction: reconciliation of biochemical and electrophysiological measurements. *Neuron* **27**, 525–537.

Lyubarsky AL, Daniele LL & Pugh EN Jr (2004). From candelas to photoisomerizations in the mouse eye by rhodopsin bleaching in situ and the light-rearing dependence of the major components of the mouse ERG. *Vision Res* **44**, 3235–3251.

Lyubarsky AL & Pugh EN Jr (1996). Recovery phase of the murine rod photoresponse reconstructed from electroretinographic recordings. *J Neurosci* **16**, 563–571.

Matthews HR (1991). Incorporation of chelator into guinea-pig rods shows that calcium mediates mammalian photoreceptor light adaptation. *J Physiol* **436**, 93–105.

Mayhew TM & Astle D (1997). Photoreceptor number and outer segment disk membrane surface area in the retina of the rat: stereological data for whole organ and average photoreceptor cell. *J Neurocytol* **26**, 53–61.

Melia TJ Jr, Cowan CW, Angleson JK & Wensel TG (1997). A comparison of the efficiency of G protein activation by ligand-free and light-activated forms of rhodopsin. *Biophys J* **73**, 3182–3191.

Nakatani K, Tamura T & Yau KW (1991*a*). Light adaptation in retinal rods of the rabbit and two other nonprimate mammals. *J General Physiol* **97**, 413–435.

Nakatani K, Tamura T & Yau KW (1991*b*). Calcium feedback and sensitivity regulation in primate rods. *J General Physiol* **98**, 95–130.

Newman EA (1989). Potassium conductance block by barium in amphibian Müller cells. *Brain Res* **498**, 308–314.

Nikonov SS, Daniele LL, Zhu X, Craft CM, Swaroop A & Pugh EN Jr (2005). Photoreceptors of $Nrl^{-/-}$ mice coexpress functional S- and M-cone opsins having distinct inactivation mechanisms. *J General Physiol* **125**, 287–304.

Nikonov S, Engheta N & Pugh EN Jr (1998). Kinetics of recovery of the dark adapted salamander photoresponse. *J General Physiol* **111**, 7–37.

Nikonov S, Lamb TD & Pugh EN Jr (2000). The role of steady phosphodiesterase activity in the kinetics and sensitivity of the light-adapted salamander rod photoresponse. *J General Physiol* **116**, 795–824.

Penn RD & Hagins WA (1972). Kinetics of the photocurrent of retinal rods. *Biophys J* **12**, 1073–1094.

Pugh E & Altman J (1988). Phototransduction. A role for calcium in adaptation. *Nature* **334**, 16–17.

Pugh EN Jr & Lamb TD (2000). Phototransduction in vertebrate rods and cones: molecular mechanisms of amplification, recovery and light adaptation. In *Handbook of Biological Physics*, vol. 3, *Molecular Mechanisms of Visual Transduction*, chap. 5, pp. 183–255. Elsevier, Amsterdam.

Reiser MA, Williams TP & Pugh EN Jr (1996). The effect of light history on the aspartate-isolated fast-PIII responses of the albino rat retina. *Invest Ophthalmol Vis Sci* **37**, 221–229.

Robinson DW, Ratto GM, Lagnado L & McNaughton PA (1993). Temperature dependence of the light response in rat rods. *J Physiol* **462**, 465–481.

Silva GA, Hetling JR & Pepperber DR (2001). Dynamic and steady-state light adaptation of mouse rod photoreceptors *in vivo*. *J Physiol* **534**, 203–216.

Tamura T, Nakatani K & Yau KW (1989). Light adaptation in cat retinal rods. *Science* **245**, 755–758.

Tamura T, Nakatani K & Yau KW (1991). Calcium feedback and sensitivity regulation in primate rods. *J Gen Physiol* **98**, 95–130.

Thomas MM & Lamb TD (1999). Light adaptation and dark adaptation of human rod photoreceptors measured from the α wave of the electroretinogram. *J Physiol* **518**, 479–496.

Tomita T & Yanagida T (1981). Origins of the ERG waves. *Vision Res* **21**, 1703–1707.

Zhang X, Wensel TG & Kraft TW (2003). GTPase regulators and photoresponses in cones of the eastern chipmunk. *J Neurosci* **23**, 1287–1297.

Acknowledgements

This work was supported by the Academy of Finland (grant 1206221). We wish to thank Ms Riitta Suoranta for expert help with the histology.